J. Chem. Thermodynamics 93 (2016) 242–254

Contents lists available at ScienceDirect

J. Chem. Thermodynamics

journal homepage: www.elsevier.com/locate/jct

Thermodynamic modelling and *in-situ* neutron diffraction investigation of the (Ce + Mg + Zn) system

Zhijun Zhu [a], Michael A. Gharghouri [b], Mamoun Medraj [c], Soo Yeol Lee [d], Arthur D. Pelton [a,*]

[a] Centre de Recherche en Calcul Thermochimique, Département de Génie Chimique, Ecole Polytechnique, Montréal, Québec, Canada
[b] Canadian Neutron Beam Centre, Canadian Nuclear Laboratories, Chalk River, Ontario, Canada
[c] Department of Mechanical Engineering, Concordia University, Montréal, Québec, Canada
[d] Department of Materials Science and Engineering, Chungnam National University, Daejeon 305-764, Republic of Korea

ARTICLE INFO

Article history:
Received 27 July 2015
Received in revised form 10 September 2015
Accepted 6 October 2015
Available online 23 October 2015

Keywords:
(Ce + Mg + Zn) system
Phase diagram
In-situ neutron diffraction
Thermodynamic assessment
Thermodynamic optimization

ABSTRACT

All available phase diagram data for the (Ce + Mg + Zn) system were critically assessed. *In-situ* neutron diffraction (ND) experiments were performed on selected samples to identify phases and transition temperatures. A critical thermodynamic evaluation and optimization of the (Ce + Mg + Zn) system were carried out and model parameters for the thermodynamic properties of all phases were obtained. The phase transformation behaviour of selected samples was well resolved from the ND experiments and experimental data were used to refine the thermodynamic model parameters.

1. Introduction

Magnesium being the lightest structural metal, Mg-based alloys have many applications. Zinc is one of the most commonly used alloying elements in Mg (AZ series), and the rare earth (RE) metals have been shown to improve creep resistance [1,2] and sheet formability (by reducing texture [3–6]).

Information on phase behaviour is essential for the design of new (RE + Mg + Zn) alloys. However, few studies of the phase diagrams and thermodynamic properties of these systems have been made. The present study was thus undertaken to better define the phase diagrams of the (RE + Mg + Zn) ternary systems through the technique of critical thermodynamic assessment and optimization coupled with limited experimentation.

In a thermodynamic optimization, adjustable model parameters are calculated using all available thermodynamic and phase-equilibrium data in order to obtain one set of model equations as functions of temperature and composition. Thermodynamic data, such as activities, can aid in the evaluation of the phase diagrams, and information on phase equilibria can be used to deduce thermodynamic properties. With this technique, it is frequently possible to resolve discrepancies in the available data. From the model equations, all of the thermodynamic properties and phase diagrams can be back-calculated, and interpolations and extrapolations can be made in a thermodynamically correct manner. The thermodynamic properties and phase diagrams are thereby rendered self-consistent and consistent with thermodynamic principles, and the available data are distilled into a small set of model parameters, ideal for computer storage. Generally, in the optimization of a ternary system one begins by optimizing the three binary sub-systems. The binary model parameters are then used to estimate the properties of the ternary phases, and these estimates are then refined by introducing ternary model parameters where required to reproduce available ternary data.

Thermodynamic evaluations and optimizations have already been reported for the binary (Mg + Zn) system [7], all binary (Mg + RE) systems [8–11] and all binary (RE + Zn) systems (as well as (Sc + Zn) and (Y + Zn) [12,13]. The liquid phase of the (Mg + Zn) system has been re-modeled in the present work with the Modified Quasichemical Model (MQM) as will be discussed in Section 4. In the present article we report on our evaluation, optimization and experimental phase diagram study of the (Ce + Mg + Zn) system. In subsequent articles, we shall report on our evaluations and optimizations of other (RE + Mg + Zn) systems as well as on our evaluation, optimization and experimental phase diagram study of the (Nd + Mg + Zn) system. As expected, all (RE + Mg + Zn) systems

* Corresponding author.

http://dx.doi.org/10.1016/j.jct.2015.10.008
0021-9614/

are very similar. The present work on the (Ce + Mg + Zn) system was greatly aided by our simultaneous assessments of all the other (RE + Mg + Zn) systems.

2. Phase equilibrium and thermodynamic data

The (Ce + Mg + Zn) system has been investigated by several authors. Different ternary phase names were used by different authors. Phases with ternary phase fields considered in the present optimization are summarized in table 1. All these phases can also be seen in the calculated isothermal section at 350 °C shown in figure 1. Our nomenclature for the ternary phases τ1 to τ7 is in agreement with that of Pavlyuk *et al.* [14]. The same nomenclature will be adopted for similar phases in other (RE + Mg + Zn) systems in our future reports. The phase Ce(Mg,Zn) in table 1 is a solid solution of CeMg and CeZn. The $CeMg_3$ and $CeMg_{12}$ phases are solid solutions with limited solubility of Zn. Although Pavlyuk *et al.* [14] and Mostafa and Medraj [20] suggested some solubility of Mg in $CeZn_3$, Ce_3Zn_{11}, $CeZn_5$, α-Ce_2Zn_{17} and $CeZn_{11}$, we have assumed that these and all other binary phases do not extend into the ternary system. The prototypes, Pearson symbols and space groups of all binary phases were given previously [7,8,12]. Although Ce_2Mg_{17} and α-Ce_2Zn_{17} have the same structure, they are treated as separate phases in the present study.

The (Ce + Mg + Zn) system was first investigated by Korol'kov and Sal'dau [16] by thermal analysis (TA). An invariant equilibrium at (341 to 343) °C was reported at a composition of 50Mg–47.5Zn–2.5Ce (wt.%). Later, an isothermal section at 300 °C was established by Mel'nik *et al.* [17] using X-ray diffraction (XRD) analysis. A total of 150 samples were studied, most of which were located in the region bounded by Mg, $MgZn_2$, CeZn and CeMg. Four ternary compounds were identified and their formulae were proposed as follows: $CeMg_7Zn_{12}$, ~$CeMg_3Zn_5$, $Ce_2Mg_3Zn_3$, and ~$Ce(Mg_{0.50-0.85}Zn_{0.5-0.15})_9$. Some of the binary and ternary compounds were reported to have limited ternary homogeneity ranges (see table 1), while CeMg and CeZn were found to form a continuous solid solution. Kolitsch *et al.* [18] reviewed all the experimental work on the (Ce + Mg + Zn) system up to the year 2000. The isothermal section at 300 °C proposed by Mel'nik *et al.* [17] was redrawn by Kolitsch *et al.* [18] to make it consistent with the accepted (Mg + Zn) binary phase diagram [19]. The four ternary compounds were denoted τ1, τ3, τ4, τ2 respectively by Kolitsch *et al.* [18]; these are the phases called τ5, τ4, τ3 and $CeMg_{12}$, respectively, in the present work.

By means of XRD, TA and scanning electron microscopy (SEM), two isopleths were established by Drits *et al.* [21] in the Mg-rich region, as shown in figure 2. Two ternary phases were also identified: $Ce(Mg_{0.9-0.5}Zn_{0.1-0.5})_{10.1}$ (believed to correspond to the $CeMg_{12}$ solid solution in the present work) and $CeMg_7Zn_{12}$ (believed to correspond to τ5 in the present work).

A ternary phase with constant Ce content of ~7.7 at.% was reported by Huang *et al.* [23,24] based on their analysis of equilibrium alloys at (350 and 400) °C. This phase is treated as $CeMg_{12}$ in the present study.

Using diffusion couple techniques, Kevorkov and Pekguleryuz [15] investigated the (Ce + Mg + Zn) phase diagram at 350 °C. Their points are shown in figure 1. These points all represent single-phase compositions [15]. Solubilities in binary and ternary solid solutions were determined by energy dispersive spectroscopy (EDS) and electron probe microanalysis (EPMA). Two new ternary compounds, called τ2 and τ6 in the present work, were reported. The τ2 phase was denoted as ~$Ce_2Mg_{53}Zn_{45}$ while τ6 was reported to be a solid

TABLE 1
Phases with ternary phase fields in the (Ce + Mg + Zn) system.

Phase name	Prototype–Pearson symbol–space group	Thermodynamic model*	
Ce(Mg,Zn)	CsCl–cP2–$Pm\bar{3}m$ [14]	(Ce,Mg)(Mg,Zn)	CeMg and CeZn form continuous solution [14,15,17,20]
$CeMg_3$	BiF_3–cF16–$Fm\bar{3}m$ [14]	(Ce,Mg)(Mg,Zn)$_3$	Reported Zn solubility 30 at.% at 300 °C [17] Reported Zn solubility 36 at.% at 350 °C [15] Reported Zn solubility 40 at.% at 197 °C [14] Reported Zn solubility 28.4 at.% at 300 °C [20]
$CeMg_{12}$	$Mn_{12}Th$–tI26–I4/mmm [14]	Ce(Mg,Zn)$_{12}$	Reported as ~$Ce(Mg_{0.50-0.85}Zn_{0.5-0.15})_9$ [17] τ2 in Ref. [18] with Zn content up to 45 at.% Reported as phase 1, with Zn content 0 to 48.49 at.% at 350 °C[15], $Ce(Mg_{0.9-0.5}Zn_{0.1-0.5})_{10.1}$ in Ref. [21] Reported as $Ce(Mg_{0.9-0.5}Zn_{0.1-0.5})_{10.1}$ [22] Reported Zn solubility 44.5 at.% at 197 °C [14] Reported Zn solubility 43.6 at.% at 350 and 400 °C [23,24] Reported Zn solubility 39.4 at.% at 300 °C [20]
τ1	$Al_{11}La_3$–oI28–Immm [25]	$Ce_3Zn_9(Mg,Zn)_2$	Reported as τ1 with Zn content 64.3 to 69 at.% [14] Reported as τ1 ($Ce_6Mg_3Zn_{19}$) [20]
τ2	Unknown	$Ce_2Mg_{53}Zn_{45}$	Assumed stoichiometric in present study Phase 2 in Ref. [15], τ2 in Ref. [14] Reported as τ2 ($CeMg_{29}Zn_{25}$) [20]
τ3	$MnCu_2Al$–cF16–Fm3 m [14,26]	CeMg(Mg,Zn)$_2$	Reported as τ3 in Ref. [14] with Zn content 38 to 50 at.% Phase 3 in Ref. [15] with proposed Zn content 45 to 50 at.% Phase 3 in Ref. [17] with Zn content 35 to 45 at.% Reported as τ3 in Ref. [18] Reported as τ3 in Ref. [20] with Zn content 35 to 52 at.%
τ4	$TbCu_7$–hP8–P6/mmm [14]	$Ce_2Mg_5Zn_9$	Assumed stoichiometric in present study Phase 2 in Ref. [17], τ3 in Ref. [18] Phase 4 in Ref. [15], τ4 in Refs. [14] and [20]
τ5	$Ce_3Mg_{13}Zn_{30}$–hP92–$P6_3/mmc$ [14]	$Ce_3Mg_{13}Zn_{30}$	Assumed stoichiometric in present study. Phase 1 in Ref. [17], τ1 in Ref. [18], phase 5 in Ref. [15], τ5 in Refs. [14] and [20] $CeMg_7Zn_{12}$ in ref [21]
τ6	Unknown	$Ce_6Mg_{11}Zn_{83}$	Assumed stoichiometric in present study Phase 6 in Ref. [15], τ6 in Refs. [14] and [20]
τ7	$Ce_{20}Mg_{19}Zn_{81}$–cF480–F43 m [27]	$Ce_{20}Mg_{19}Zn_{81}$	Assumed stoichiometric in present study, τ6 in Ref. [14] Reported as τ7 [20]

* Elements within brackets substitute on the same sublattice.

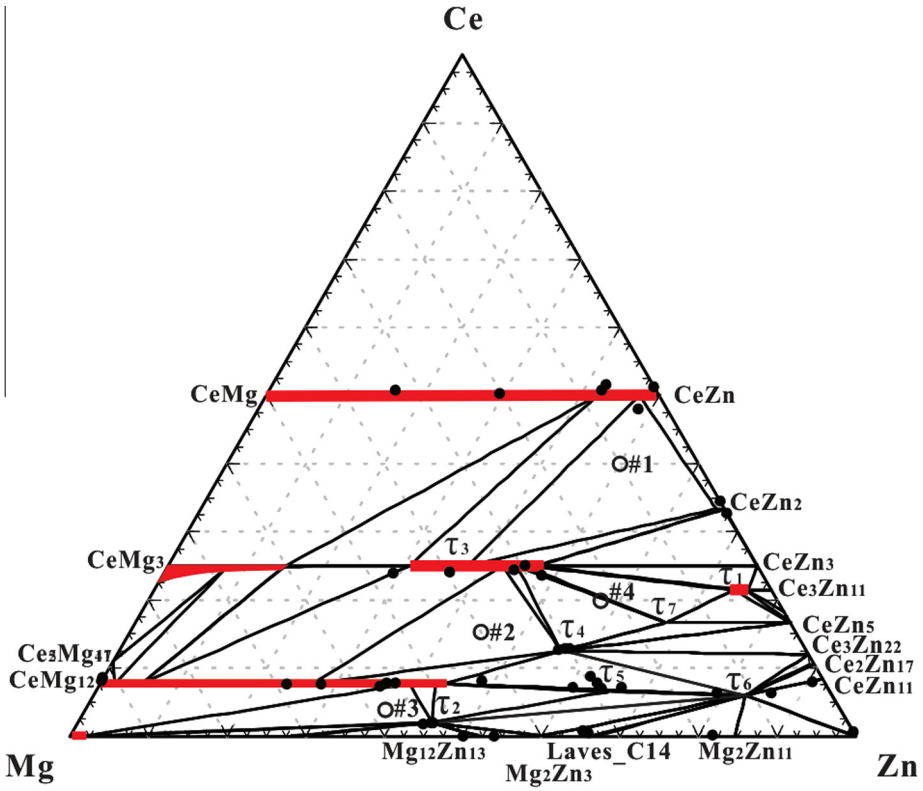

FIGURE 1. Calculated optimized isothermal section (mole fraction) of the (Ce + Mg + Zn) system at 350 °C showing data points of Kevorkov and Pekguleryuz [15] which indicate single-phase regions. Compositions of the four samples used in the present ND experiments are also shown.

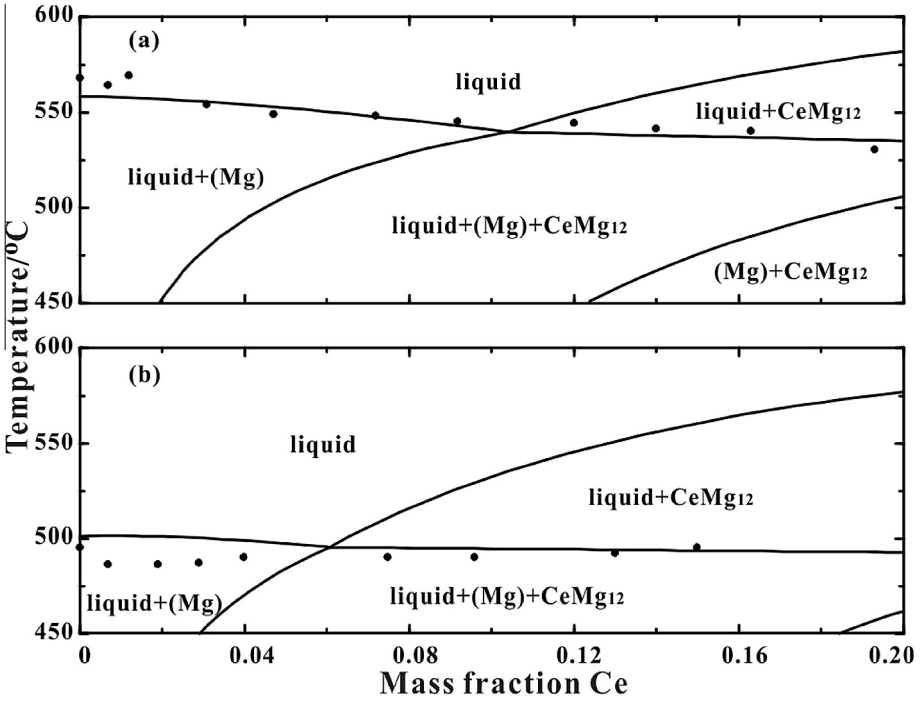

FIGURE 2. Calculated optimized isopleths with constant Zn content of 24 wt.% (a) and 34 wt.% (b) in the (Ce + Mg + Zn) system showing points from Drits *et al.* [21].

solution with constant Ce content of ~6 at.% and Mg content of (~7.5 to 14.5) at.%. Due to its limited solubility and unknown crystal structure, τ6 is assumed to be a stoichiometric phase in the present work as shown in table 1. The $Ce(Mg_{0.9-0.5}Zn_{0.1-0.5})_{10.1}$ phase reported in Ref. [22] was shown to be part of the $CeMg_{12}$ solution which can dissolve Zn up to 48.49 at.% according to the EDS measurements.

The (Ce + Mg + Zn) system was later investigated by Chiu *et al.* [28]. Ten samples were prepared and studied by Differential Scanning Calorimetry (DSC). However, only data from Mg-rich samples

were interpreted by the authors. Some of the tie-triangles were experimentally validated but no details of the experiments were given. Their results will be shown later in Section 5.

An isothermal section at 197 °C was later constructed by Pavlyuk *et al.* [14] using XRD, wavelength dispersive spectrometry (WDS) and EPMA. Their diagram will be shown later in Section 5. A total of 53 samples were prepared covering the entire ternary composition range. All ternary compounds reported by Kevorkov and Pekguleryuz [15] were confirmed. In addition, two new compounds were identified: $Ce_3(Zn_{0.863}Mg_{0.137})_{11}$ and $Ce_{20}Mg_{19}Zn_{81}$ (τ1 and τ7 in the present work). Although $Ce_3(Zn_{0.863}Mg_{0.137})_{11}$ and Ce_3Zn_{11} have the same structural prototype, Pavlyuk *et al.* [14] treated them as two separate phases. They argued that the lattice parameters of these two phases differ significantly and a sample consisting of these two phases at equilibrium was observed.

The isothermal section at 300 °C was recently investigated by Mostafa and Medraj [20] over the entire composition range using diffusion couples. Their reported isothermal section [20] is shown later in figure 6(a). All the ternary phases reported by Pavlyuk *et al.* [14] were confirmed. In addition, the ternary solution phase proposed by Huang *et al.* [23,24] was also reported, but its crystal structure was not resolved.

Based on the available experimental data from the literature, the following phases with ternary phase fields are considered in the present work (see figure 1 and table 1).

Ce(Mg,Zn): The CeMg and CeZn binary phases both have the CsCl structure and in all reported isothermal sections [14,15,17,20] they form a continuous solution. The reported lattice constant of CeMg at room temperature is 0.3898 nm [29] and that of CeZn is 0.3696 nm [30], while that of the Ce(Mg,Zn) solution is 0.3730 nm at 40 at.%Zn and 0.384 nm at 10 at.%Zn [14]. The Ce content is nearly constant at 50 at.%. Consequently, the model (Ce,Mg)(Mg,Zn) was chosen in the present optimization, in which Mg and Zn substitute on one sublattice while Ce occupies a second sublattice. A small amount of Mg can also occupy the RE sublattice, as evidenced by the slight solubility of Mg in REMg as considered previously [8–11].

$CeMg_3$: Zn can substitute for Mg in $CeMg_3$ [14,15,17,20]. Consequently, the model $(Ce,Mg)(Mg,Zn)_3$ is used. The phase has the same structure as $CeMg_3$. The solubility of Zn in $CeMg_3$ as reported by different authors is summarized in table 1. The lattice constant of binary $CeMg_3$ was reported to be 0.7443 nm [31], decreasing with increasing Zn content to 0.7077 nm at 40 at.%Zn [14] which is due to the smaller atomic radius of Zn compared to Mg.

$CeMg_{12}$: A ternary phase with approximately the same mole fraction of Ce ($\sim Ce(Mg_{0.50\text{-}0.85}Zn_{0.5\text{-}0.15})_9$ [17], Ce $(Mg_{0.9\text{-}0.5}Zn_{0.1\text{-}0.5})_{10.1}$ [21], a ternary phase with ~7.7 at.% Ce [23,24] and τ8 in ref [20]) was reported by several investigators who treated the ternary phase and $CeMg_{12}$ as separate phases. However, other investigators reported [14,15,28] that the ternary phase is actually continuous with $CeMg_{12}$ (see figure 1). This point is still a subject of controversy. In the present work, we have found that one continuous phase with the model $Ce(Mg,Zn)_{12}$ is most consistent with all the data.

τ1: The structural prototype of both τ1 and the Ce_3Zn_{11} binary phase is $Al_{11}La_3$. However, Pavlyuk *et al.* [14] showed that they have been observed to coexist and their lattice constants differ significantly; the lattice constant of τ1, when extrapolated to the binary composition of Ce_3Zn_{11}, does not coincide with that of Ce_3Zn_{11}. Hence, in the present work, we treat them as two separate phases. In the $Al_{11}La_3$ prototype there are 6 distinct sites: 2*a*, 2*c*, 4*g*, 4*j* and two 8*l* sites [32], the 2*a* and 4*g* sites being occupied by La. The crystal structure of τ1 was resolved by Pavlyuk *et al.* from single crystal data [25]: the 2*a* and 4*g* sites are occupied solely by Ce (Ce does not enter the other sites, thereby giving a constant Ce mole fraction); the two 8*l* sites are occupied solely by Zn and the 2*c* and 4*j* sites can be occupied by Mg and Zn. However, since the lowest Zn content reported by Pavlyuk *et al.* [14] was 64.2 at.%, which is the case when the 2*c* and the two 8*l* sites are fully occupied by Zn and the 4*j* sites are fully occupied by Mg, the model $Ce_2Zn_2Ce_4(Mg,Zn)_4Zn_8Zn_8$ (simplified to $Ce_3Zn_9(Mg,Zn)_2$) seems more reasonable for τ1.

τ2: This phase was reported as phase 2 by Kevorkov and Pekguleryuz [15], as τ2 by Pavlyuk *et al.* [14], and as τ2 ($CeMg_{29}Zn_{25}$) by Mostafa and Medraj [20]. The crystal structure remains unknown. EDS measurements [15] gave a composition of $Ce_{1.82}Mg_{53.14}Zn_{45.04}$ in good agreement with EPMA measurements [14], which gave a composition of $Ce_{1.8}Mg_{53.1}Zn_{45.1}$. No solubility information on this phase can be found. Consequently, it is treated in the present work as a stoichiometric compound, with the suggested formula $Ce_2Mg_{53}Zn_{45}$.

τ3: The τ3 phase was first reported by Mel'nik *et al.* [17] with a lattice constant of 0.7064 nm. The prototype was reported to be either $MgLi_2Ag$ or $AlMnCu_2$. The crystal structure was later resolved by Pavluyk *et al.* [14,26]; the prototype was determined from single crystal X-ray diffraction measurements to be $AlMnCu_2$ with a lattice constant ranging from (0.7035 to 0.7036) nm depending on the Zn content. Given that the maximum Zn content of this phase is reported as 50 at.% [14,15], 45 at.% [17], or 52 at.% [20], the model $CeMg(Mg,Zn)_2$ is used in the present work.

τ4, τ5, τ6 and τ7: Although some limited solubility is reported for these four phases [14,15,17,20], they are treated in the present work as stoichiometric phases, with suggested stoichiometries $Ce_2Mg_5Zn_9$, $Ce_3Mg_{13}Zn_{30}$, $Ce_6Mg_{11}Zn_{83}$, and $Ce_{20}Mg_{19}Zn_{81}$, respectively, based on the reported compositions. The crystal structures of τ4 and τ5 were obtained by Pavlyuk *et al.* [14] from XRD powder diffraction data while that of τ7 was resolved from single crystal data [27]. The crystal structure of τ6 remains unknown.

It may be noted that phases similar to all the ternary phases shown in table 1 have been observed in several other (RE + Mg + Zn) systems with the exception of the τ1, τ2, τ6 and τ7 phases. However, investigations have not been carried out in the composition regions where these four phases appear in any system other than the (Ce + Mg + Zn) and (Nd + Mg + Zn) systems (τ1, τ2, and τ7 were reported in the (Nd + Mg + Zn) system [33]).

3. Experimental investigation

In-situ neutron diffraction (ND) was used in the present work to investigate the phase transformation behaviour in order to validate and refine the thermodynamic modelling.

Neutron diffraction data were acquired using the C2 powder diffractometer of the Canadian Neutron Beam Centre, located at the National Research Universal (NRU) reactor, Canadian Nuclear Laboratories (CNL). Diffraction from the (531) reflection of a silicon single crystal monochromator produced incident neutrons with a nominal wavelength of 0.133 nm. The C2 diffractometer is equipped with an 800-channel detector covering an 80° range in scattering angle 2θ, allowing multiple diffraction peaks to be acquired simultaneously.

The four sample compositions shown in figure 1 and table 1 were selected based on preliminary optimizations of the isothermal phase diagram at 300 °C. Sample compositions corresponding to three-phase regions were chosen as they were expected to exhibit the greatest number of transitions, thereby providing the most information.

All samples were prepared from Ce (99.9 wt.%, STREM Chemicals Inc., Newburyport, MA, USA), Mg (99.8 wt.%, CANMET Materials Technology Laboratory, Ottawa, ON, Canada) and Zn (99.9 wt.%, Alfa Aesar, Haverhill, MA, USA) in an induction furnace under an argon atmosphere. Crucibles were made from 0.15 mm thick Ta foil with a purity of 99.5 wt.%. All samples were melted three times to

improve homogeneity. ICP tests (Inductively Coupled Plasma mass spectrometry) showed that Zn losses of 5 wt.% by vaporization occurred during melting. Consequently, an excess of 5 wt.% Zn was added before melting.

Figure 3 shows the furnace used for the NPD experiments. Two infrared lamps were used to heat the samples. Crucibles were made of 304 stainless steel for samples #1, #2 and #3. For sample #4, a Ta crucible was required because of the high melting point. The use of a Ta crucible also simplified the analysis of the diffraction patterns since Ta has fewer diffraction peaks than stainless steel. Stainless steel, however, is less expensive. An eccentrically loaded motor was attached to the top of the furnace to vibrate the sample in order to weaken preferred orientation and to avoid super-cooling that occurred during preliminary tests performed without vibrating the sample. All the ND experiments were carried out under a flowing Ar atmosphere. The mass of the samples varied from 10 g to 20 g.

In an *in-situ* ND experiment, diffraction patterns are acquired as a function of temperature as a specimen is heated or cooled. Each crystallographic phase in the specimen produces a distinct set of diffraction peaks, with the intensity of each diffraction peak proportional to the quantity of the corresponding phase in the specimen. During cooling or heating, a transition temperature is thus the temperature at which the diffraction peaks for a given phase first appear or completely disappear. Due to limitations in the sensitivity of the technique, diffraction peaks for new phases are typically not detectable until the temperature is somewhat below or above the equilibrium transition temperature. In order to quantify the offset associated with the sensitivity of the method, heating and cooling ND measurements on pure Mg were carried out. The apparent melting temperature of pure Mg was determined to be 640 °C upon heating and 635 °C upon cooling. The accepted melting temperature of pure Mg is 650 °C [34]. Hence, all reported temperatures shown in the present report have been corrected by 15 °C because only *in-situ* data collected during cooling were analysed.

Several samples were prepared for preliminary tests. ICP measurements were performed on these samples before and after the ND experiments. It was found that the change in composition during the ND experiments was very limited, typically less than 2 at.% for any component.

XRD was also performed to identify the phases present in the as-cast alloys. The information obtained from XRD was used as a starting point to index the subsequent ND results. Rietveld analysis

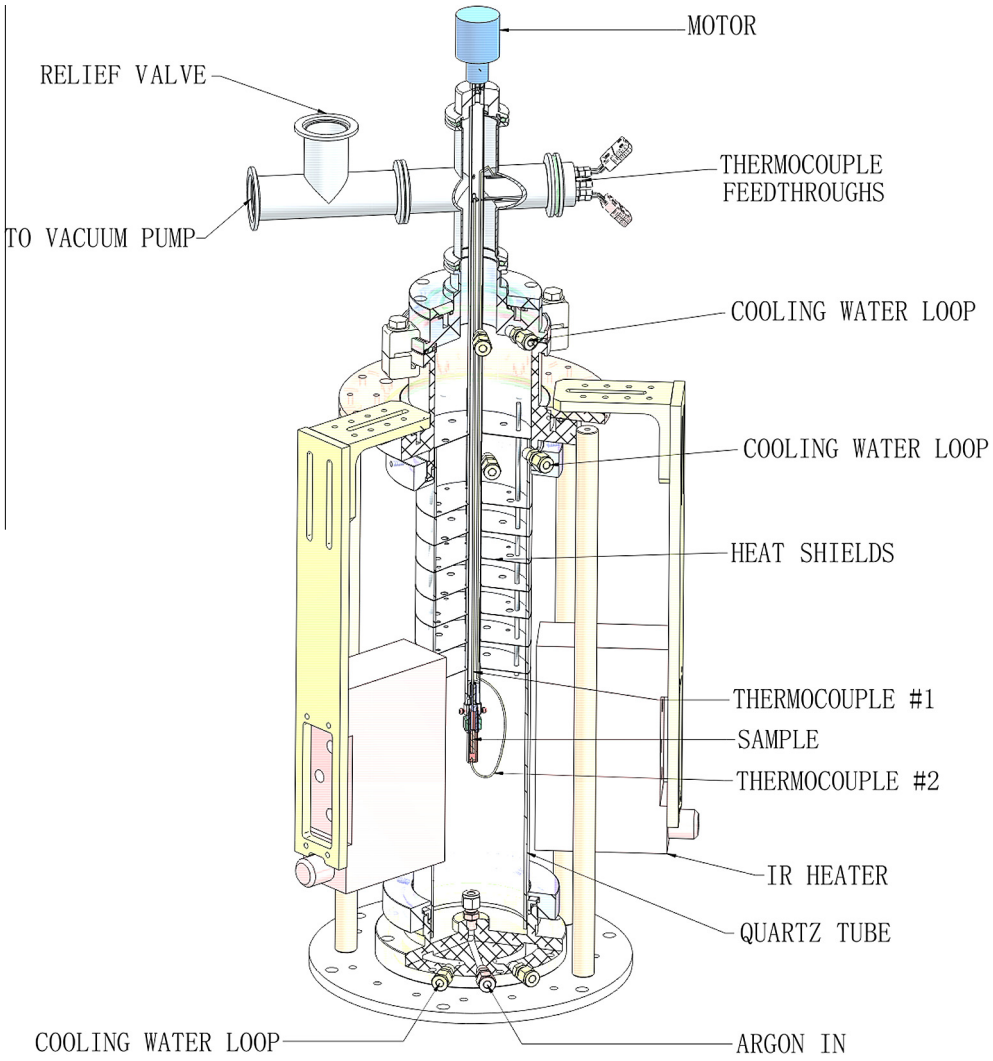

FIGURE 3. Schematic drawing of the furnace used for the ND experiments.

TABLE 2
Sample compositions and transition temperatures measured in NPD experiments.

Sample No.	Composition (at.%)	Transition temperatures (±2.5 °C)	Phase first appearing below this temperature
#1	$Ce_{40}Mg_{10}Zn_{50}$	735 °C	$CeZn_2$
		720 °C	Ce(Mg,Zn)
		665 °C	τ3
#2	$Ce_{16}Mg_{40}Zn_{44}$	700 °C	τ3
		615 °C	τ1
		550 °C	$CeMg_{12}$
#3	$Ce_4Mg_{58}Zn_{38}$	555 °C	$CeMg_{12}$
		455 °C	τ6?
		365 °C	(Mg), hcp
#4	$Ce_{20}Mg_{22}Zn_{58}$	730 °C	τ1
		710 °C	τ3

? Possible phase.

was performed on the ND patterns as well as the XRD patterns using the GSAS/EXPGUI software [35]. Transition temperatures obtained from the ND experiments are summarized in table 2.

In the ND experiments it was found from initial tests that the intensity of the diffraction peaks for newly precipitated phases stabilized very quickly (within 3 min) as the temperature changed. Consequently, in later experiments, diffraction patterns were recorded at intervals of 5 °C, with an acquisition time of 3 min at each temperature. In this way, relatively accurate transformation temperatures could be obtained within a reasonable amount of beam time.

3.1. Sample #1 ($Ce_{40}Mg_{10}Zn_{50}$)

Figure 4(a) shows ND patterns for sample #1 obtained upon cooling. Although patterns were acquired every 5 °C, only a few selected patterns are shown. A hump around $2\theta = 30°$ due to the liquid phase is visible at 765 °C. All other peaks above background at this temperature correspond to the crucible or the thermocouples, indicating that the sample was entirely in the liquid state at 765 °C. Patterns for 735 °C, 720 °C and 665 °C were obtained just after the appearance of a new phase. Analysis of the patterns shows that $CeZn_2$ is the first phase to appear upon cooling at 735 °C, followed by Ce(Mg,Zn) at 720 °C and τ3 at 665 °C. The diffraction peaks corresponding to these precipitating phases are weak but discernible, despite the short acquisition time (3 min). The pattern at 645 °C shows no new peaks compared with those observed at 665 °C. The derived transition temperatures for sample #1 are shown on figure 5(a).

The room temperature lattice constant of the Ce(Mg,Zn) phase was 0.3712 nm which is closer to that of CeZn (0.3696 nm [30]) than that of CeMg (0.3898 nm [29]), consistent with the phase relationships in figure 1.

3.2. Sample #2 ($Ce_{16}Mg_{40}Zn_{44}$)

ND patterns at selected temperatures for sample #2 are shown in figure 4(b). The primary phase for this sample is τ3, which forms at 700 °C. τ1 appears at 615 °C and $CeMg_{12}$ is first detected at 550 °C. At 370 °C, no new peaks other than those at 550 °C were are observed. Phases τ3 and τ1 have their strongest diffraction peak at $2\theta = \sim 30°$, making the analysis difficult. Furthermore, diffraction peaks from the sample are much weaker than those from the crucible and thermocouple, further complicating the analysis. The measured transition temperatures for sample #2 are shown on figure 5(b).

3.3. Sample #3 ($Ce_4Mg_{58}Zn_{38}$)

ND patterns at selected temperatures for sample #3 are shown in figure 4(c). The first phase that appears upon cooling is $CeMg_{12}$ which forms at 555 °C. At 505 °C, no additional peaks are observed. At 455 °C, a weak diffraction peak appears on the shoulder of the strong stainless steel peak at a scattering angle of ~37°. The diffraction peak could not be indexed, but we believe it to correspond to τ6, which would be consistent with our thermodynamic analysis. Peaks from the hcp (Mg) phase are first observed at 365 °C. The measured transition temperatures for sample #3 are shown on figure 5(c).

The lattice constants of $CeMg_{12}$ measured for sample #3 ($a = b = 0.9592$ nm; $c = 0.5608$ nm) are smaller than those measured in sample #2 ($a = b = 0.9791$ nm; $c = 0.5616$ nm). Since the atomic size of Zn is smaller than that of Mg, this result indicates a higher content of Zn in sample #3 than in sample #2 in agreement with the phase relationships in figure 1.

3.4. Sample #4 ($Ce_{20}Mg_{22}Zn_{58}$)

Figure 4(d) shows selected ND patterns for $Ce_{20}Mg_{22}Zn_{58}$. Analysis of the patterns shows that only two phases were observed to form during cooling with τ1 forming below 730 °C and τ3 below 710 °C. The τ3 peak at $2\theta = \sim 30°$ is very strong, indicating preferred orientation. The measured transition temperatures for sample #4 are shown in figure 5(d).

Our refined values for the lattice constants of the τ3 phase for samples #1, 2 and 4 were nearly identical (0.7049(0), 0.7049(8) and 0.7048(5) nm respectively), indicating that the compositions of this phase are very similar in the three samples, in agreement with the phase relationships shown in figure 1.

3.5. Thermodynamic optimizations

Thermodynamic data for the pure elements were given previously [7,8,12]. The optimized thermodynamic model parameters of the three binary sub-systems were taken from Ansara *et al.* [7] (Mg + Zn), Kang *et al.* [8] (Ce + Mg) and Zhu and Pelton [12] (Ce + Zn).

For the three binary sub-systems, the Modified Quasichemical Model (MQM) [36,37], which takes account of short-range ordering (SRO), was used to model the liquid phase. Consequently, the MQM is used to model the substantial amount of SRO in the liquid phase in the ternary system. For details of the model, see references [12,13,36,37]. The symmetric (Kohler-like) model [37] was used to estimate the properties of the ternary liquid phase from the optimized binary model parameters. No additional ternary model parameters were introduced.

In the optimization of the (Mg + Zn) binary system, Ansara *et al.* [7] did not use the MQM for the liquid phase. Consequently, the liquid phase was remodelled by Spencer [7] using the MQM, keeping the same parameters as Ansara *et al.* for all other (Mg + Zn) binary phases. The "coordination numbers", which are MQM model parameters, were set to

$$Z^{Mg}_{Mg,Zn} = Z^{Zn}_{Mg,Zn} = Z^{Mg}_{Mg,Mg} = Z^{Zn}_{Zn,Zn} = 6 \quad (1)$$

and the MQM model parameters were introduced as

$$\Delta g_{MgZn} = -6778 + 3.138\,T/K + (-1966 + 2.008)X_{MgMg} + (-3975 + 1.6736)X_{ZnZn}\,(J/g\text{-atom}) \quad (2)$$

The binary Bcc_A2, Fcc_A1 and Hcp_A3 solutions are described by a substitutional solution model as discussed previously [12].

As shown in table 1, Mg and Zn can substitute for each other on one or two sublattices in some phases (τ1, τ3, Ce(Mg,Zn), $CeMg_3$, $CeMg_{12}$). These phases are modelled with the Compound Energy

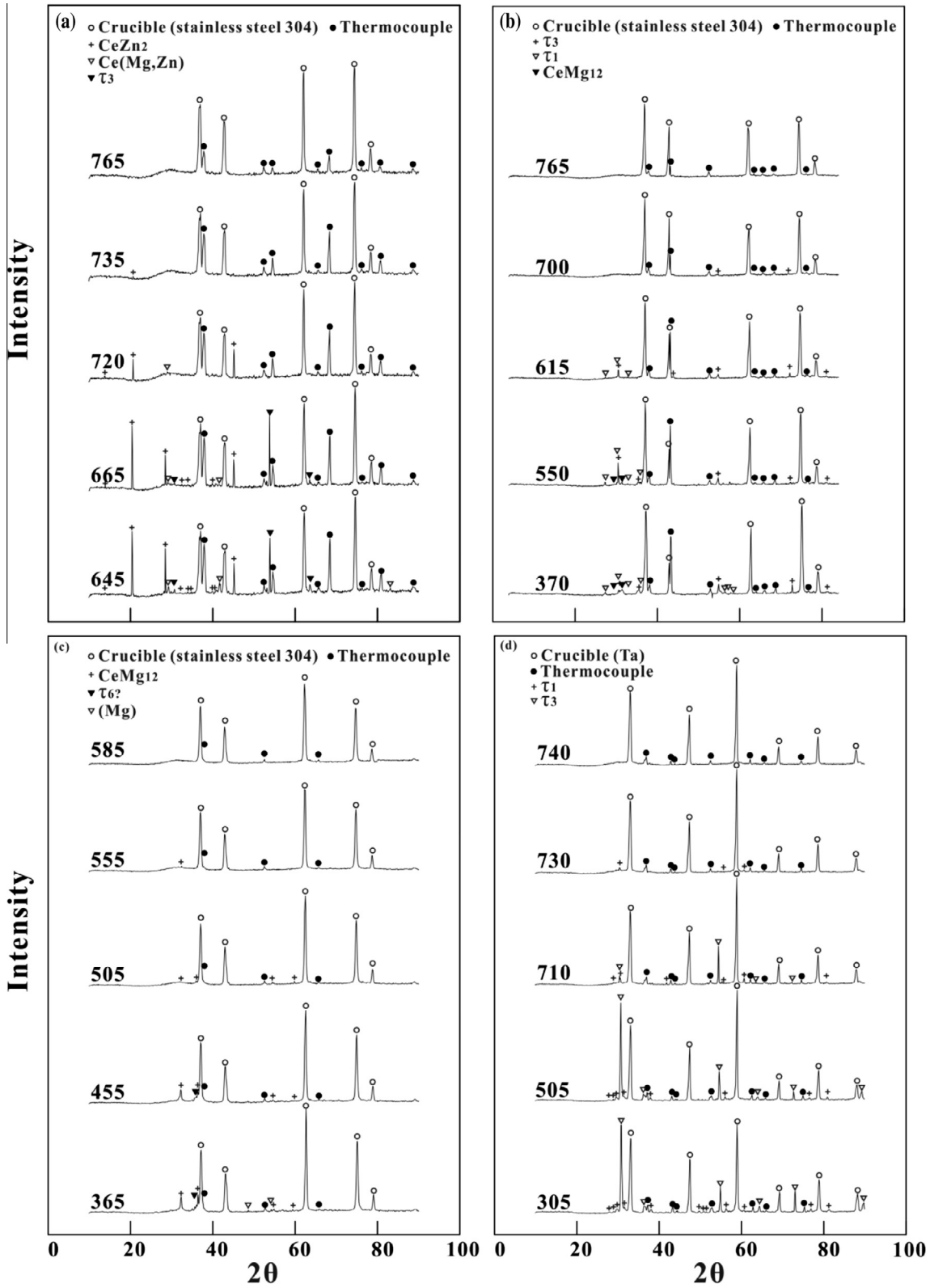

FIGURE 4. Selected ND patterns for (a) $Ce_{40}Mg_{10}Zn_{50}$, (sample #1), (b) $Ce_{16}Mg_{40}Zn_{44}$, (sample #2), (c) $Ce_{4}Mg_{58}Zn_{38}$, (sample #3) and (d) $Ce_{20}Mg_{22}Zn_{58}$, (sample #4).

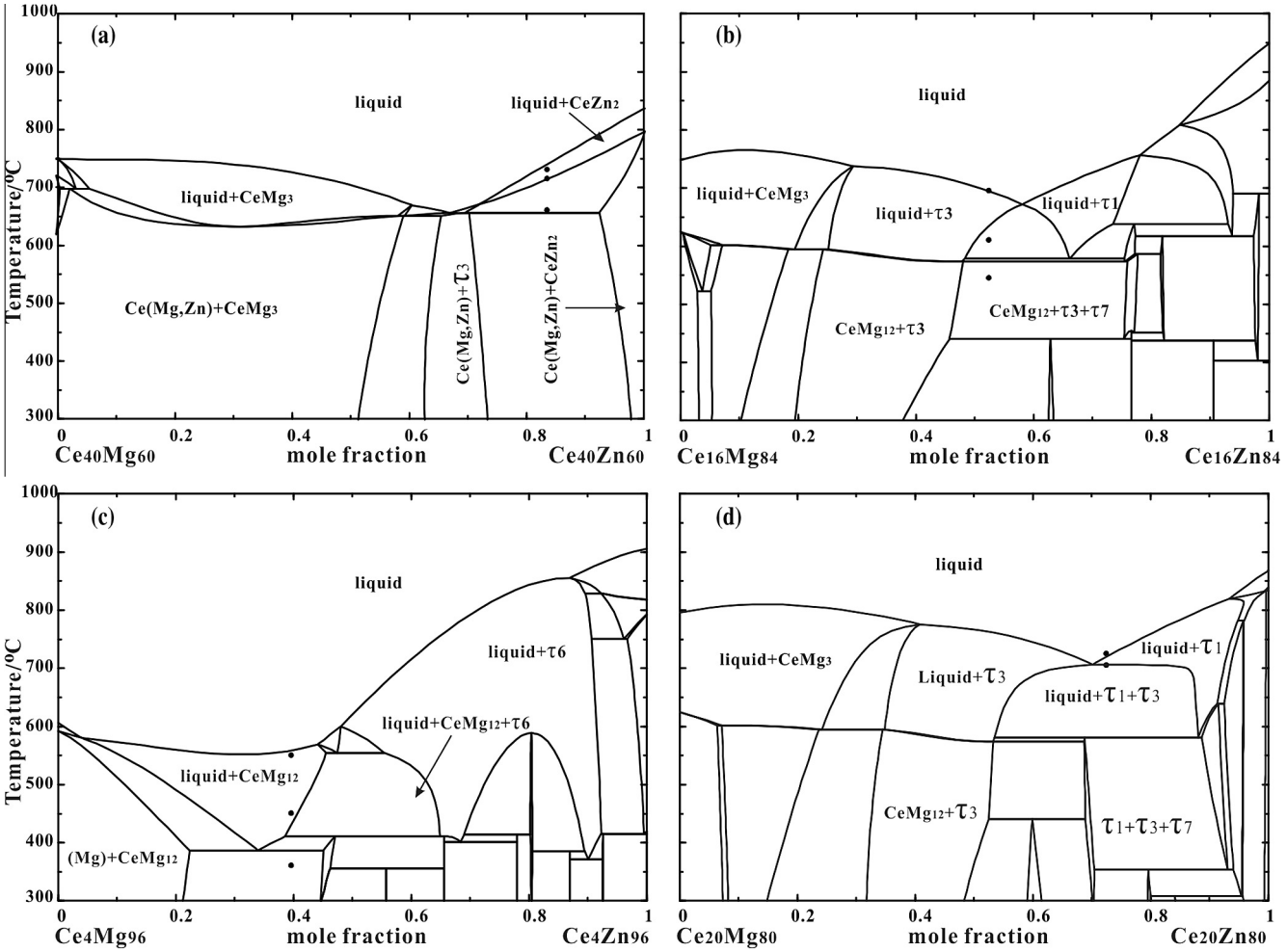

FIGURE 5. Calculated optimized isopleths of the (a) $Ce_{40}Mg_{60}$–$Ce_{40}Zn_{60}$, (b) $Ce_{16}Mg_{84}$–$Ce_{16}Zn_{84}$, (c) Ce_4Mg_{96}–Ce_4Zn_{96} and (d) $Ce_{20}Mg_{80}$–$Ce_{20}Zn_{80}$ sections showing experimental transition temperatures from samples #1, #2, #3 and #4, respectively.

Formalisim (CEF) [38]. For example, the Gibbs energy of the Ce(Mg, Zn) phase according to the model (Ce,Mg)(Mg,Zn) (per mole of formula) can be expressed as follows:

$$\begin{aligned} G^{(Ce,Mg)(Mg,Zn)} &= y'_{Ce}y''_{Mg}G^{0,(Ce,Mg)(Mg,Zn)}_{Ce:Mg} + y'_{Ce}y''_{Zn}G^{0,(Ce,Mg)(Mg,Zn)}_{Ce:Zn} \\ &+ y'_{Mg}y''_{Mg}G^{0,(Ce,Mg)(Mg,Zn)}_{Mg:Mg} + y'_{Mg}y''_{Zn}G^{0,(Ce,Mg)(Mg,Zn)}_{Mg:Zn} \\ &+ RT\left(y'_{Ce}ln\, y'_{Ce} + y'_{Mg}ln\, y'_{Mg}\right) \\ &+ RT\left(y''_{Mg}ln\, y''_{Mg} + y''_{Zn}ln\, y''_{Zn}\right) \\ &+ \sum_i L^i_{Ce,Mg:Mg}\left(y'_{Ce} - y'_{Mg}\right)^i y'_{Ce}y'_{Mg}y''_{Mg} \\ &+ \sum_i L^i_{Ce,Mg:Zn}\left(y'_{Ce} - y'_{Mg}\right)^i y'_{Ce}y'_{Mg}y''_{Zn} \\ &+ \sum_i L^i_{Ce:Mg,Zn}\left(y''_{Mg} - y''_{Zn}\right)^i y'_{Ce}y''_{Mg}y''_{Zn} \\ &+ \sum_i L^i_{Mg:Mg,Zn}\left(y''_{Mg} - y''_{Zn}\right)^i y'_{Mg}y''_{Mg}y''_{Zn} \\ &+ L_{Ce,Mg:Mg,Zn}y'_{Ce}y'_{Mg}y''_{Mg}y''_{Zn} \end{aligned} \quad (3)$$

where y'_{Ce} and y'_{Mg} are the site fractions of Ce and Mg in the first sublattice and y''_{Mg} and y''_{Zn} are the site fractions of Mg and Zn in the second sublattice, $G^{0,(Ce,Mg)(Mg,Zn)}_{Ce:Mg}$, $G^{0,(Ce,Mg)(Mg,Zn)}_{Ce:Zn}$, $G^{0,(Ce,Mg)(Mg,Zn)}_{Mg:Mg}$ and $G^{0,(Ce,Mg)(Mg,Zn)}_{Mg:Zn}$ are the Gibbs energies of the end-members (CeMg, CeZn, MgMg and MgZn) at temperature T under the convention that the enthalpies of the elements are equal to zero in their stable states at $T = 298.15$ K, and $L^i_{Ce,Mg:Mg}$, $L^i_{Ce,Mg:Zn}$, $L^i_{Ce:Mg,Zn}$, $L^i_{Mg:Mg,Zn}$ and $L_{Ce,Mg:Mg,Zn}$ are interaction parameters to be optimized. The Gibbs energies of τ1, τ3, $CeMg_3$ and $CeMg_{12}$ can be expressed similarly.

The τ2, τ4, τ5, τ6 and τ7 phases are treated as stoichiometric compounds.

No thermodynamic properties for the ternary compounds could be found in the literature. To obtain initial estimates of the enthalpies and entropies of formation of the ternary compounds, three lines passing through the compound on the ternary Gibbs triangle were drawn parallel to the three edges of the triangle. The six intersection points of these lines with the edges defined six binary compositions whose enthalpies and entropies calculated from the binary model parameters were then averaged to give the initial estimates. Thereafter, these values were adjusted to best reproduce the available data.

All model parameters optimized in the present work are listed in table 3. All other model parameters (apart from the MQM parameters for liquid (Mg + Zn) shown in Section 4) have been given previously [7,8,12]. Very few model parameters are required. The enthalpies of formation of all compounds have reasonable values. The entropies of formation are all small and negative.

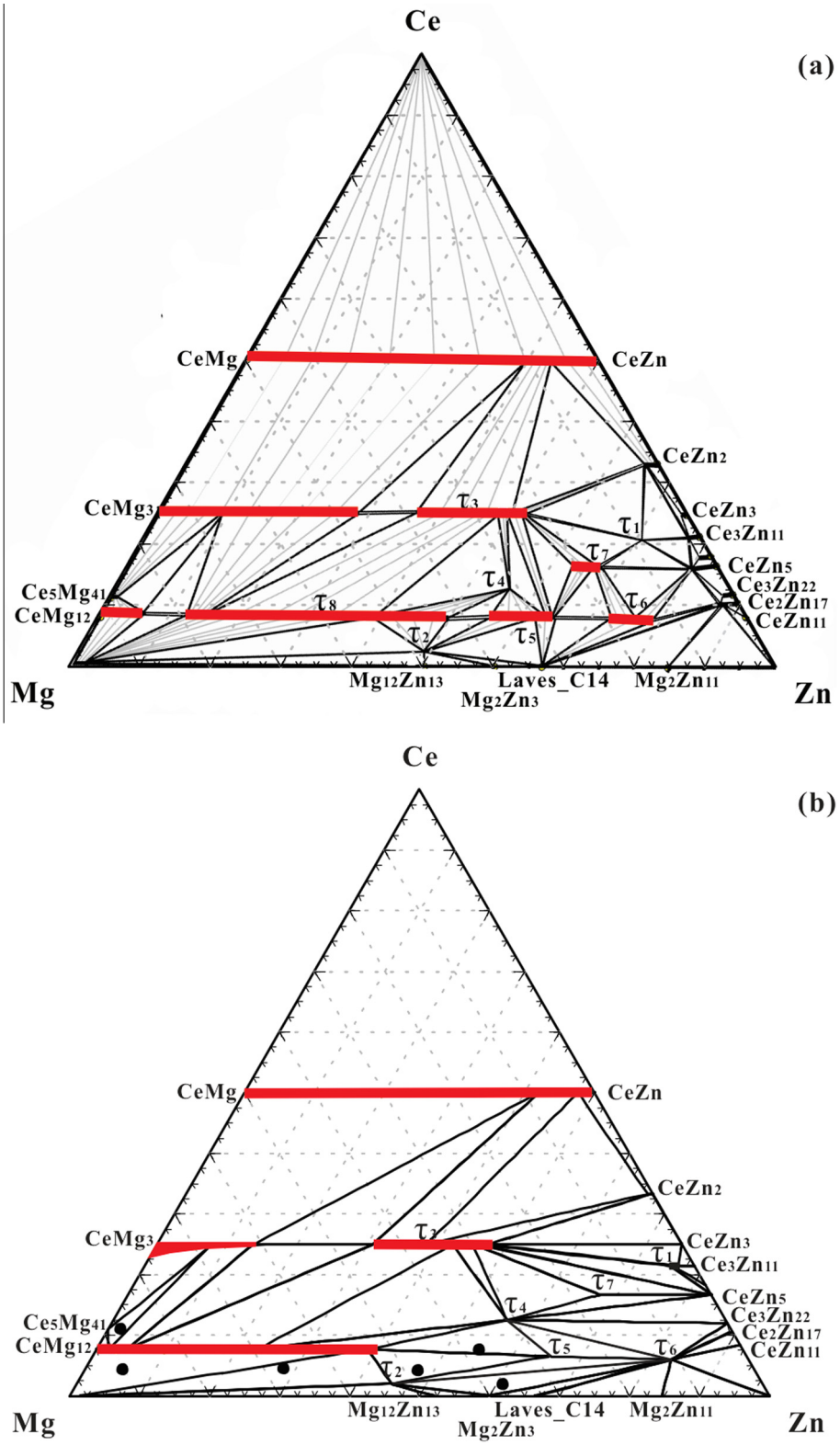

FIGURE 6. (a) Reported [20] and (b) calculated optimized isothermal section (mole fraction) of the (Ce + Mg + Zn) system at 300 °C showing experimental data points identified by Chiu *et al.* [28] as lying in three-phase regions.

4. Comparison of calculations with experimental values

The calculated isothermal section at 350 °C, including the experimental data from Kevorkov and Pekguleryuz [15], is shown in figure 1. All compositions identified as lying in single-phase regions are reproduced as such. Reported compositions [15] corresponding to the single-phase regions of τ2, τ4, τ5 and τ6 are not reproduced exactly since these four ternary phases were treated as stoichiometric compounds in the present work.

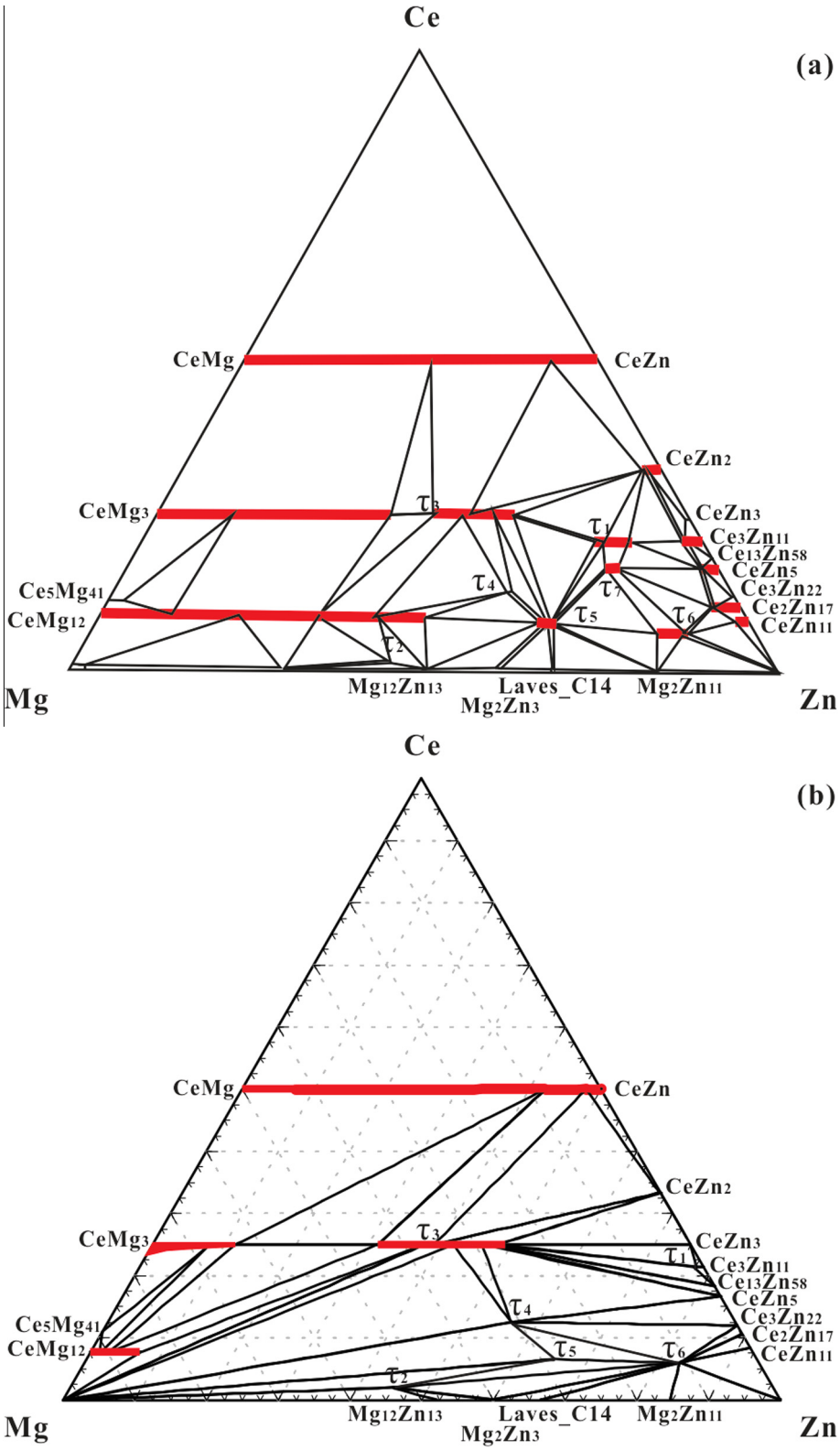

FIGURE 7. (a) Reported [14] and (b) calculated optimized isothermal section (mole fraction) of the (Ce + Mg + Zn) system at 197 °C.

Figure 6(b) shows the calculated isothermal section at 300 °C along with points which Chiu *et al.* [28] identified as lying in three-phase regions. All these tie-triangles were reproduced in the present work. The region containing the data point corresponding to the highest Mg content was mistakenly interpreted as a three-phase region in ref [28]. The more recently reported isothermal section at 300 °C from Mostafa and Medraj [20] is shown in figure 6(a). As expected, the reported solubility ranges of some of

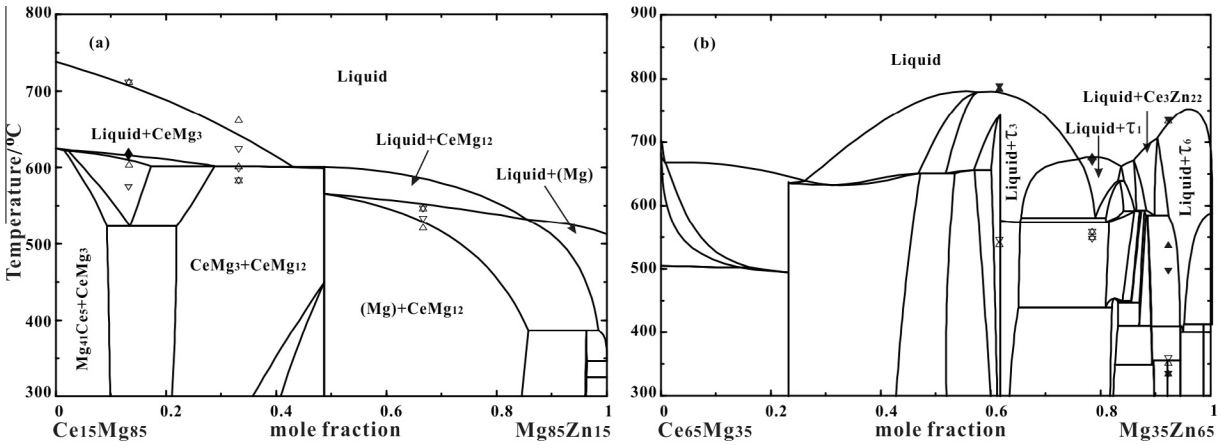

FIGURE 8. Calculated optimized isopleths of the (a) $Ce_{15}Mg_{85}$–$Mg_{85}Zn_{15}$ and (b) $Ce_{65}Mg_{35}$–$Mg_{35}Zn_{65}$ sections showing data points of Chiu *et al.* [28]. ▲ strong heating signal; ▼ strong cooling signal; △ weak heating signal; ▽ weak cooling signal.

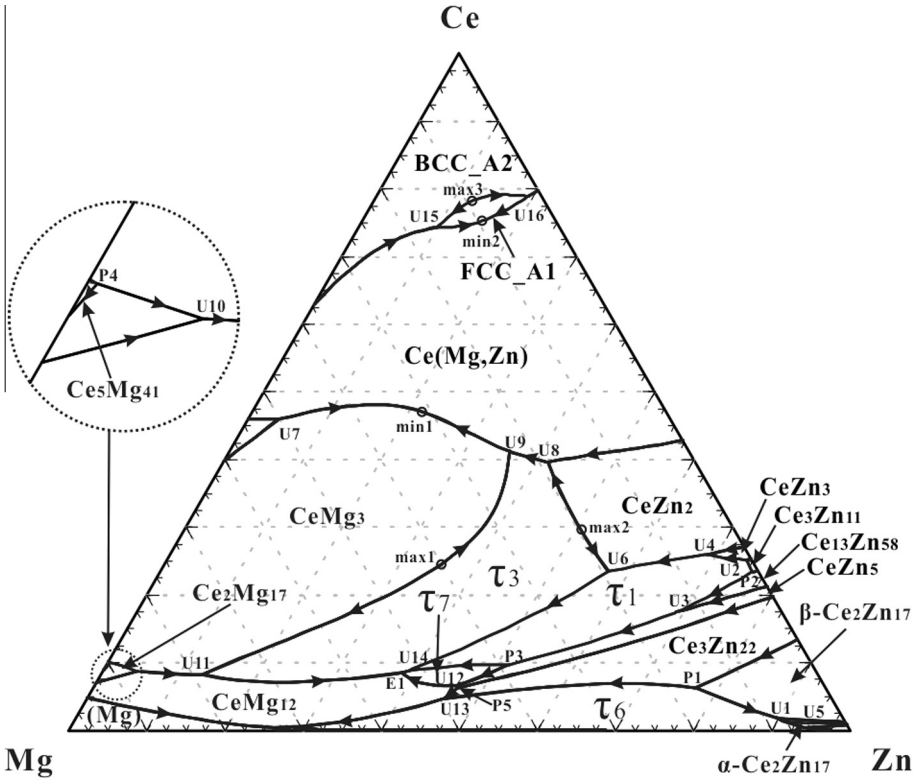

FIGURE 9. Tentative calculated *liquidus* projection for (Ce + Mg + Zn) system (mole fraction).

the ternary phases are not reproduced because we treated these phases as stoichiometric compounds. The proposed phase relationships in the Zn-rich region were also not all reproduced.

In the optimizations, more weight was given to the experimental data from the present ND experiments because these experiments were performed at higher temperatures and in the presence of the liquid phase; hence, equilibrium is more likely to be attained.

Reported [14] and calculated isothermal sections at 197 °C are shown in figure 7. The solubility of Zn in the $CeMg_{12}$ phase is calculated as ~8 at.%, which is much less than that reported in ref [14] (44.5 at.%). Furthermore, the τ7 phase is not stable at 197 °C according to the calculations. It was not possible to reproduce all the experimental data from the present ND experiments while also reproducing the reported large Zn solubility in $CeMg_{12}$ and maintaining τ7 stable at 197 °C. The samples of Pavlyuk *et al.* [14] were annealed at 197 °C for four weeks which may have been insufficient to reach equilibrium at such a low temperature. That their system was not completely at equilibrium is supported by their observation of $Mg_{51}Zn_{20}$, which is metastable [7]. As mentioned above, more weight was given to the current high temperature ND results in the optimization.

Calculated Zn solubilities in $CeMg_3$ are less than those reported at 350 °C, 300 °C and 197 °C. The ND results proved incompatible

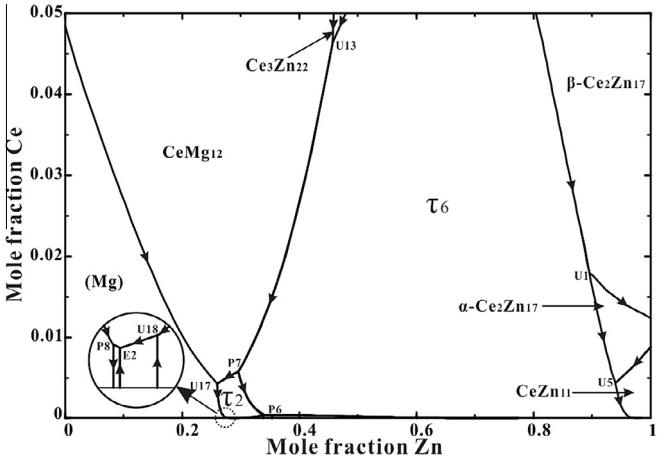

FIGURE 10. Enlargement of part of figure 9.

TABLE 3
Thermodynamic model parameters optimized in the present work for the (Ce + Mg + Zn) system.

Phase name	Model	Parameters (J · g-atom^{-1})
Ce(Mg,Zn)	(Ce,Mg)(Mg,Zn)	$L^{0,Ce(Mg,Zn)}_{Ce:Mg,Zn} = -4812$
$CeMg_3$	(Ce,Mg)(Mg,Zn)$_3$	$G^{0,CeMg_3}_{Ce:Zn} = -34204 + 5.23\,T$/K
		$L^{0,CeMg_3}_{Ce:Mg,Zn} = -4184$
		$L^{1,CeMg_3}_{Ce:Mg,Zn} = -2092$
$CeMg_{12}$	Ce(Mg,Zn)$_{12}$	$L^{0,CeMg_{12}}_{Ce:Mg,Zn} = -2248$
τ1	Ce_3Zn_9(Mg,Zn)$_2$	$G^{0,\tau1}_{Ce:Zn:Mg} = -31380 + 2.99\,T$/K
		$G^{0,\tau1}_{Ce:Zn:Zn} = -36334 + 6.45\,T$/K
τ2	$Ce_2Mg_{53}Zn_{45}$	$G^{0,\tau2}_{Ce:Mg:Zn} = -10547 + 0.92\,T$/K
τ3	Ce(Mg,Zn)$_2$Mg	$G^{0,\tau3}_{Ce:Mg:Mg} = -19000 + 6.63\,T$/K
		$G^{0,\tau3}_{Ce:Zn:Mg} = -34037 + 6.28\,T$/K
		$L^{0,\tau3}_{Ce:Mg,Zn:Mg} = 1046$
		$L^{1,\tau3}_{Ce:Mg,Zn:Mg} = 4184$
τ4	$Ce_2Mg_5Zn_9$	$G^{0,\tau4}_{Ce:Mg:Zn} = -25724 + 5.23\,T$/K
τ5	$Ce_3Mg_{13}Zn_{30}$	$G^{0,\tau5}_{Ce:Mg:Zn} = -20465 + 3.94\,T$/K
τ6	$Ce_6Mg_{11}Zn_{83}$	$G^{0,\tau6}_{Ce:Mg:Zn} = -23389 + 4.89\,T$/K
τ7	$Ce_{20}Mg_{19}Zn_{81}$	$G^{0,\tau7}_{Ce:Mg:Zn} = -30193 + 4.20\,T$/K

with the higher solubilities and, again, more weight was given to the ND results, which are more likely to correspond to true equilibrium conditions due to the presence of the liquid phase.

Two calculated isopleths with constant Zn contents of 24 and 34 wt.% are shown in figure 2 along with experimental TA data from Drits *et al.* [21]. The experimental points [21] at low Ce contents cannot be reproduced since they are in disagreement with the accepted *liquidus* in the (Mg + Zn) binary system.

Figure 8 shows calculated optimized isopleths along with the DTA data of Chiu *et al.* [28]. The data are reasonably well reproduced.

Chiu *et al.* [28] proposed a thermodynamic optimization of the system. However, they focused mainly on Mg-rich compositions and included only three ternary compounds. Their optimization reproduced the values shown in figure 8(a) reasonably well, but not the data in figure 8(b).

Calculated isopleths are shown in figure 5 along with experimental data from the present ND experiments. Calculated transition temperatures and precipitation sequences are in good agreement with the experiments. The higher transition temperatures (especially the *liquidus* temperatures) are considered more reliable than the lower transition temperatures because of kinetic constraints on attaining equilibrium at low temperature.

A tentative calculated *liquidus* projection for the (Ce + Mg + Zn) system is shown in figures 9 and 10 and a tentative list of the calculated temperatures of invariant reactions, maxima and minima is given in table 4.

As mentioned in Section 2, an invariant equilibrium at (341 to 343) °C was reported by Korol'kov and Sal'dau [16], which could correspond to U18, P8 or E2, the most likely being E2 because eutectic reactions are the most easily detected by thermal analysis.

5. Discussion

In the optimization, greater weight was accorded to the ND data from the present investigation, firstly because the ND data were obtained in situ at equilibrium at higher temperatures, and secondly because, due to the high penetrating power of neutrons, large samples 10 g to 20 g could be used, thereby leading to better control of composition and increased resistance to oxidation.

In subsequent articles we shall report on thermodynamic modelling and ND experiments in the (Nd + Mg + Zn) system as well as thermodynamic optimizations of most other ternary (RE + Mg + Zn) systems [39,40,41]. The model parameters will be included in the FTlite light metals database of the FactSage database computing system [42] which already contains optimized model parameters for the solid and liquid phases of a large number of binary and ternary Mg- and Al-containing systems. Through the models, the properties and phase equilibria of multicomponent systems can thus be estimated and calculated.

All calculations in the present work were performed with the FactSage software [42].

6. Conclusions

All available phase diagram data for the (Ce + Mg + Zn) system were critically assessed. *In-situ* neutron diffraction (ND) experiments were performed on selected samples to identify phases and transition temperatures. A critical thermodynamic evaluation and optimization of the (Ce + Mg + Zn) system was carried out and model parameters for the thermodynamic properties of all phases were obtained. The phase transformation behaviour of selected samples was well resolved from the ND experiments and experimental data were used to refine the thermodynamic model parameters.

TABLE 4
Tentative calculated invariant reactions, maxima and minima and their temperatures (°C) in the (Ce + Mg + Zn) system.

	t/°C		t/°C		t/°C		t/°C		t/°C		t/°C
P1	849	P2	833	U1	818	U2	816	U3	781	U4	775
U5	751	U6	709	U7	697	U8	656	U9	650	P3	639
P4	622	U10	601	U11	594	P5	592	U12	591	U13	584
U14	580	E1	574	U15	502	U16	498	P6	413	P7	410
U17	386	U18	351	P8	346	E2	346	max1	~782	max2	~743
max3	~533	min1	~632	min2	~484						

All optimized model parameters from the present work are summarized in table 3. Binary parameters were reported in previous articles [7,8,12]. Very few model parameters are required, and all parameters have thermodynamically reasonable values. In particular, no additional ternary parameters were required in the MQM model for the liquid phase.

Acknowledgements

This research was supported by funding from the Natural Sciences and Engineering Research Council of Canada (NSERC) Magnesium Strategic Research Network (Grant number: NETGP 340821-06). More information on the Network can be found at www.MagNET.ubc.ca. The authors would like to thank Dr. Dmytro Kevorkov and Dr. Ahmad Mostafa for helping prepare the samples. SYL was supported by the National Research Foundation of Korea (NRF) grant funded by the Korean government (MSIP) (No. 2013R1A1A1076023).

References

[1] B.L. Mordike, T. Ebert, Magnesium: properties — applications — potential, Mat. Sci. Eng. A-Struct. 302 (2001) 37–45.
[2] I.P. Moreno, T.K. Nandy, J.W. Jones, J.E. Allison, T.M. Pollock, Microstructural stability and creep of rare-earth containing magnesium alloys, Scr. Mater. 48 (2003) 1029–1034.
[3] J. Bohlen, M.R. Nürnberg, J.W. Senn, D. Letzig, S.R. Agnew, The texture and anisotropy of magnesium-zinc-rare earth alloy sheets, Acta Mater. 55 (2007) 2101–2112.
[4] R.K. Mishra, A.K. Gupta, P.R. Rao, A.K. Sachdev, A.M. Kumar, A.A. Luo, Influence of cerium on the texture and ductility of magnesium extrusions, Scr. Mater. 59 (2008) 562–565.
[5] N. Stanford, M.R. Barnett, The origin of "rare earth" texture development in extruded Mg-based alloys and its effect on tensile ductility, Mat. Sci. Eng. A-Struct. 496 (2008) 399–408.
[6] K. Hantzsche, J. Bohlen, J. Wendt, K.U. Kainer, S.B. Yi, D. Letzig, Effect of rare earth additions on microstructure and texture development of magnesium alloy sheets, Scr. Mater. 63 (2010) 725–730.
[7] I. Ansara, A.T. Dinsdale, M.H. Rand, COST 507: definition of thermochemical and thermophysical properties to provide a database for the development of new light alloys, Thermochemical database for light metal alloys, vol. 2, Office for Official Publications of the European Communities, Luxembourg, 1998; P. Spencer, unpublished work.
[8] Y.-B. Kang, L. Jin, P. Chartrand, A.E. Gheribi, K. Bai, P. Wu, Thermodynamic evaluations and optimizations of binary Mg-light rare Earth (La, Ce, Pr, Nd, Sm) systems, CALPHAD 38 (2012) 100–116.
[9] Y.-B. Kang, A. Pelton, P. Chartrand, P. Spencer, C. Fuerst, Critical evaluation and thermodynamic optimization of the binary systems in the Mg–Ce–Mn–Y system, J. Phase Equilib. Diff. 28 (2007) 342–354.
[10] Y.-B. Kang, A.D. Pelton, P. Chartrand, C.D. Fuerst, Critical evaluation and thermodynamic optimization of the Al–Ce, Al–Y, Al–Sc and Mg–Sc binary systems, CALPHAD 32 (2008) 413–422.
[11] Y.-B. Kang, unpublished work.
[12] Z. Zhu, A. Pelton, Critical assessment and optimization of phase diagrams and thermodynamic properties of RE–Zn systems-part I: Sc–Zn, La–Zn, Ce–Zn, Pr–Zn, Nd–Zn, Pm–Zn and Sm–Zn, J. Alloys Compd. 641 (2015) 249–260.
[13] Z. Zhu, A. Pelton, Critical assessment and optimization of phase diagrams and thermodynamic properties of RE–Zn systems-Part II: Y-Zn, Eu–Zn, Gd–Zn, Tb–Zn, Dy–Zn, Ho–Zn, Er–Zn, Tm–Zn, Yb–Zn and Lu–Zn, J. Alloys Compd. 641 (2015) 261–271.
[14] V. Pavlyuk, B. Marciniak, E. Różycka-Sokołowska, The isothermal section of the phase diagram of Ce–Mg–Zn ternary system at 470 K, Intermetallics 20 (2012) 8–15.
[15] D. Kevorkov, M. Pekguleryuz, Experimental study of the Ce–Mg–Zn phase diagram at 350 °C via diffusion couple techniques, J. Alloys Compd. 478 (2009) 427–436.
[16] A.M. Korol'kov, P.Y. Sal'dau, Solubility of zinc and cerium in magnesium in the solid state, Izv. Sekt. Fiz.-Khim. Anal., Inst. Obshch. Neorg. Khim., Akad. Nauk SSSR, 16 (1946) 295–306.
[17] E.V. Mel'nik, M.F. Kostina, Ya.P. Yarmlyuk, O.F. Zmii, Study of magnesium–zinc–cerium and magnesium–zinc–calcium ternary systems, Magnievye Splavy, Mater. Vses. Soveshch. Issled., Razrab. Primen. Magnievyhk Splavov, (1978) 95–99.
[18] U. Kolitsch, P. Bellen, S. Kaesche, D. Macciò, N. Bochvar, Y. Liberov, P. Rogl, G. Effenberg, G. Petzow, Ternary Alloys–A Comprehensive Compendium of Evaluated Constitutional Data and Phase Diagrams, 17, Weinheim: VCH Verlagsgesellschaft, MSI GmbH, Stuttgart, Germany, 2000. 168–176.
[19] R. Agarwal, S.G. Fries, H.L. Lukas, G. Petzow, F. Sommen, T.G. Chart, G. Effenberg, Assessment of the Mg–Zn system, Z. Metallkd. 83 (1992) 216–223.
[20] A. Mostafa, M. Medraj, Phase equilibria of the Ce–Mg–Zn ternary system at 300 °C, Metals 4 (2014) 168–195.
[21] M.E. Drits, E.I. Drozdova, I.G. Korol'kova, V.V. Kinzhibalo, A.T. Tyvanchuk, Investigation of polythermal sections of the Mg–Zn–Ce system in the Mg-rich region, Russ. Metall-Metall-U (1989) 195–197.
[22] M.E. Drits, E.I. Drozdova, I.G. Korol'kova, V.V. Kinzhibalo, A.T. Tyvanchuk, Polythermal sections of the magnesium–zinc–cerium system in the magnesium-rich region, Izv. Akad. Nauk SSSR, Met. (1989) 198–200.
[23] M.-I. Huang, H.-X. Li, H. Ding, Y.-P. Ren, G.-W. Qin, S.-M. Hao, Partial phase relationships of Mg–Zn–Ce system at 350 °C, Trans. Nonferr. Metal. Soc. 19 (2009) 681–685.
[24] M.-L. Huang, H.-X. Li, H. Ding, L. Bao, X.-B. Ma, S.-M. Hao, Intermetallics and phase relations of Mg–Zn–Ce alloys at 400 °C, Trans. Nonferr. Metal. Soc. 22 (2012) 539–545.
[25] V. Pavlyuk, E. Rozycka-Sokolowska, B. Marciniak, The new ternary phases of $La_3(Zn_{0.874}Mg_{0.126})_{11}$ and $Ce_3(Zn_{0.863}Mg_{0.137})_{11}$, Acta Crystallogr. C 66 (2010) i25–i28.
[26] V. Pavlyuk, P. Solokha, G. Dmytriv, B. Marciniak, V. Paul-Boncour, The Heusler-type alloy $MgZn_2Ce$, Acta Crystallogr. E 63 (2007) i161.
[27] V. Pavlyuk, P. Solokha, O. Zelinska, V. Paul-Boncour, A. Nowik-Zajac, $Ce_{20}Mg_{19}Zn_{81}$: A new structure type with a giant cubic cell, Acta Crystallogr. C 64 (2008) i50–i52.
[28] C.-N. Chiu, J. Gröbner, A. Kozlov, R. Schmid-Fetzer, Experimental study and thermodynamic assessment of ternary Mg–Zn–Ce phase relations focused on Mg-rich alloys, Intermetallics 18 (2010) 399–405.
[29] H. Nowotny, The crystal structures of Ni_5Ce, Ni_5La, Ni_5Ca, Cu_5La, Cu_5Ca, Zn_5La, Zn_5Ca, MgCe, MgLa and MgSr, Z. Metallkd. 34 (1942) 247–253.
[30] Y. Uwatoko, K. Suenaga, G. Oomi, X-ray diffraction study of the structural change in cerium-zinc (CeZn) under high pressure, J. Magn. Magn. Mater. 104–107 (1992) 645–646.
[31] G. Berger, A. Weiss, Ternary intermetallic phases with Heusler-phase-type structure in the system Ag–Mg–RE (RE ≡ La, Ce, Pr, Nd, Sm), J. Less-common Met. 142 (1988) 109–121.
[32] A.H. Gomes de Mesquita, K.H.J. Buschow, The crystal structure of so-called α-$LaAl_4$ (La_3Al_{11}), Acta Crystallogr. 22 (1967) 497–501.
[33] H. Xu, J. Fan, H.-L. Chen, R. Schmid-Fetzer, F. Zhang, Y. Wang, Q. Gao, T. Zhou, Experimental determination of the phase equilibria of the Mg–Nd–Zn system at 320 °C, J. Alloys Compd. 603 (2014) 100–110.
[34] W.M. Haynes (Ed.), CRC Handbook of Chemistry and Physics, ninety-fifth ed., (Internet Version 2015), CRC Press/Taylor and Francis, Boca Raton, FL.
[35] B. Toby, EXPGUI, a graphical user interface for GSAS, J. Appl. Crystallogr. 34 (2001) 210–213.
[36] A. Pelton, S. Degterov, G. Eriksson, C. Robelin, Y. Dessureault, The modified quasichemical model I—Binary solutions, Metall. Mater. Trans. B 31 (2000) 651–659.
[37] A. Pelton, P. Chartrand, The modified quasi-chemical model: Part II. Multicomponent solutions, Metall. Mater. Trans. A 32 (2001) 1355–1360.
[38] M. Hillert, The compound energy formalism, J. Alloys Compd. 320 (2001) 161–176.
[39] Zhijun Zhu, Michael A. Gharghouri, Arthur D. Pelton, Thermodynamic Modeling and In-situ Neutron Diffraction Investigation of the Nd-Mg-Zn system, J. Chem. Thermodyn, accepted for publication.
[40] Zhijun Zhu, Arthur D. Pelton, Thermodynamic Modeling of the La-Mg-Zn, Pr-Mg-Zn and Sm-Mg-Zn systems, J. Alloys Compd. 652 (2015) 415–425.
[41] Zhijun Zhu, Arthur D. Pelton, Thermodynamic Modeling of the Y-Mg-Zn, Gd-Mg-Zn, Tb-Mg-Zn, Dy-Mg-Zn, Ho-Mg-Zn, Er-Mg-Zn, Tm-Mg-Zn and Lu-Mg-Zn systems, J. Alloys Compd. 652 (2015) 426–443.
[42] C.W. Bale, E. Bélisle, P. Chartrand, S.A. Decterov, G. Eriksson, K. Hack, I.H. Jung, Y.B. Kang, J. Melançon, A.D. Pelton, C. Robelin, S. Petersen, FactSage thermochemical software and databases - recent developments, CALPHAD 33 (2009) 295–311. <www.factsage.com>.